Mechanism of grain growth during severe plastic deformation of a nanocrystalline Ni–Fe alloy

Cite as: Appl. Phys. Lett. **94**, 011908 (2009); https://doi.org/10.1063/1.3065025
Submitted: 23 November 2008 • Accepted: 09 December 2008 • Published Online: 07 January 2009

Y. B. Wang, J. C. Ho, X. Z. Liao, et al.

Mechanism of grain growth during severe plastic deformation of a nanocrystalline Ni–Fe alloy

Y. B. Wang,[1] J. C. Ho,[1] X. Z. Liao,[1,a)] H. Q. Li,[2] S. P. Ringer,[3] and Y. T. Zhu[4]
[1]*School of Aerospace, Mechanical & Mechatronic Engineering, the University of Sydney, New South Wales 2006, Australia*
[2]*Los Alamos National Laboratory, Los Alamos, New Mexico 87545, USA*
[3]*Australian Key Centre for Microscopy & Microanalysis, the University of Sydney, New South Wales 2006, Australia*
[4]*Department of Materials Science & Engineering, North Carolina State University, Raleigh, North Carolina 27695-7919, USA*

(Received 23 November 2008; accepted 9 December 2008; published online 7 January 2009)

Deformation induced grain growth has been widely reported in nanocrystalline materials. However, the grain growth mechanism remains an open question. This study applies high-pressure torsion to severely deform bulk nanocrystalline Ni-20 wt % Fe disks and uses transmission electron microscopy to characterize the grain growth process. Our results provide solid evidence suggesting that high pressure torsion induced grain growth is achieved primarily via grain rotation for grains much smaller than 100 nm. Dislocations are mainly seen at small-angle subgrain boundaries during the grain growth process but are seen everywhere in grains after the grains have grown large. © *2009 American Institute of Physics*. [DOI: 10.1063/1.3065025]

Severe plastic deformation (SPD) techniques have been widely used to produce bulk ultrafine-grained and nanostructured materials.[1,2] It has been well documented that deformation induced grain refinement is mainly caused by dislocation accumulation and rearrangement for materials with medium to high stacking fault (SF) energies and under low strain rates.[3–5] Twining also plays a significant role in grain refinement for materials with low SF energies and/or under very high strain rates.[6] There is always a minimum average grain size that a specific SPD condition can achieve for a specific material and this minimum size is a function of not only the intrinsic material properties (e.g., SF energy)[7,8] but also the extrinsic processing parameters.[8] One of the reasons that produce this minimum grain size is that SPD processes also result in grain growth. The minimum grain size is achieved by the dynamic balance between the grain refinement process and the grain growth process.

Plastic deformation induced grain growth has been widely reported in various plastic deformation processes including nanoindentation,[9] high pressure torsion,[10] uniaxial tension,[11,12] and uniaxial compression.[13] The grain growth changes the structures of nanocrystalline (nc) materials and therefore will no doubt affect their mechanical properties. Molecular dynamics simulations[14,15] and theoretical analysis[16] have been carried out to understand the mechanisms of deformation induced grain growth and contradictory results have been reported. Sansoz and Dupont[14] show that stress-driven nc grain growth results mainly from rotation of nanograins and propagation of shear bands while Farkas *et al.*[15] suggest that, for grains having the same size as those presented in Ref. 14, grain boundary migration is responsible for the nc grain growth. Experimental results obtained via *in situ* transmission electron microscopy (TEM) investigations suggested that deformation induced grain growth can be realized via grain rotation and grain boundary sliding for grains of ~10 nm.[17,18] However, the results remain controversial[19] and the thin film effect of TEM samples, in which grains are constrained only in two dimensions, on the deformation/grain growth behavior of nc grains cannot be ruled out. Recent *in situ* TEM investigation of relatively thick freestanding Al films presents another deformation induced grain growth mechanism—stress coupled grain-boundary migration; i.e., a grain grows at the expense of other neighboring grains.[20] The mechanism of stress coupled grain-boundary migration was observed in grains larger than 100 nm. This raises a question: Does the same mechanism also apply to bulk nc grains with grain sizes much smaller than 100 nm? If the answer is no, a further question is raised: What is the grain growth mechanism that operates in bulks with grains much smaller than 100 nm? To answer these questions, we have applied the high-pressure torsion (HPT) technique to severely deform *bulk* nc Ni-20 wt % Fe disks and used TEM to characterize the material before and after the deformation.

The NiFe alloy used in this investigation was produced via electrochemical deposition.[21] Disks with thickness around 0.7 mm and diameter of 10 mm were processed using HPT for one, two, and nine revolutions, respectively, under 3.8 GPa at room temperature and a very low strain rate of about 10^{-2} s^{-1}. TEM thin foils were prepared by cutting $\phi 3$ mm disks from near the edges of the HPT disks, grinding them to about 100 μm thickness and then electropolishing them using a solution of nitric acid and methanol (1:3) at −30 °C. TEM observations were carried out in a Philips CM12 microscope working at 120 keV and a JEOL 3000F microscope operating at 300 keV.

Figure 1 shows TEM images of the as-received sample (a) and the one-revolution HPT sample [(b) and (c)]. The grain sizes in the as-received sample are in the range of 5–50 nm with the average size of ~22 nm. Most grains are equiaxed while some are elongated with length to width aspect ratios around 2. Careful examination of grain orientations reveals that neighboring grains normally have very different orientations, as evidenced in the diffraction contrast image in Fig. 1(a), in which it is difficult to find neighboring grains

a)Electronic mail: xliao@usyd.edu.au.

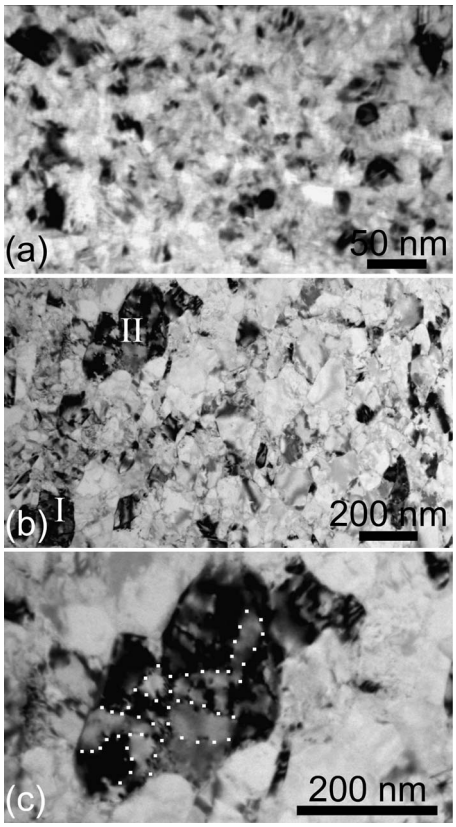

FIG. 1. (a) A diffraction contrast image of the as-received Ni–Fe sample; (b) a diffraction contrast image of the one-revolution HPT sample. Two large grains with dark contrast showing subgrains with slightly different contrast are marked with "I" and "II," respectively; (c) a magnified image of the grain marked with "II" in (b). Some small angle subgrain boundaries are highlighted with dotted lines.

having dark contrast simultaneously. Significant grain growth was achieved after one-revolution HPT as shown in Fig. 1(b). The grain sizes are in the range of 40–250 nm with the average grain size of ~95 nm. One significant feature in the microstructure of this sample is that many subgrains with small angle subgrain boundaries are seen within each grain. This can be easily seen when a large grain is in a strong diffraction condition (i.e., the orientation of the grain is on or close to a major zone axis, e.g., ⟨110⟩) so that the grain appears dark with each subgrain within the grain having slightly different contrast in a bright-field TEM image and the subgrain boundaries are seen clearly. Two examples of large grains formed by subgrains with small angle subgrain boundaries seen in Fig. 1(b) are marked with "I" and "II," respectively. Grain II is further magnified in Fig. 1(c). Some of the small angle subgrain boundaries of large subgrains in Fig. 1(c) are highlighted by dotted lines. Because the sizes of many subgrains are consistent with those seen in the as-received sample, it indicates that large grains were formed through the rotation of the initial smaller grains. Note that the grain boundary of the large dark contrast grain in Fig. 1(c) is of irregular shape that matches the boundaries of the initial smaller grains, indicating that no grain boundary migration occurred at this stage of the grain growth.

Figure 2(a) shows another example of a large grain (~80 nm) formed by several subgrains with small angle subgrain boundaries. The small angle boundaries decorated with dislocations are highlighted with dotted lines. Figure 2(b) shows a high-resolution TEM image of the area marked with a white rectangle in Fig. 2(a), in which part of a small angle grain boundary is included. Misorientation of ~6° between the two sides of the boundary is seen clearly by drawing two straight lines, with each parallel to a group of {111} in each subgrain, respectively. Two edge-on dislocations at the subgrain boundary are marked with white "T." Note that one side of the grain boundary in Fig. 2(a), marked by two black arrowheads, is very straight, indicating that, in addition to grain rotation, some grain boundary migration and rearrangement also occurred during the grain growth process.

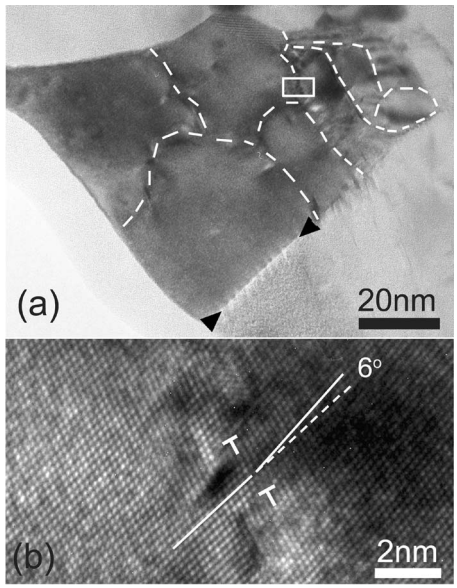

FIG. 2. (a) A TEM image of a grain having subgrains with small angle subgrain boundaries which are highlighted with dotted lines; (b) a high-resolution TEM image of the area marked with a white rectangle in (a), showing 6° lattice misalignment across a subgrain boundary. Two dislocations located at the subgrain boundary are marked with white "T."

Small angle grain boundaries can be seen not only among grains along the HPT disk plane but also among grains along the direction perpendicular to the plane, i.e., parallel to the electron beam direction in TEM, indicating that the grain rotation occurred in all three dimensions. An example is shown in Fig. 3(a), in which Moiré fringes caused by the small angle misorientation of neighboring grains along the TEM electron beam direction are seen. The Moiré fringes form a domain structure, some of which are circled with dotted white lines in Fig. 3(a). Each domain has its own fringe orientation and the domain sizes are around 20 nm, which is consistent with the original grain sizes in the as-received sample. One domain area marked with "A" in Fig. 3(a) is further magnified and shown in Fig. 3(b). The spacing of the Moiré fringes is slightly larger than 1 nm and corresponds to 11° misorientation between the upper and lower subgrains. Figure 3(c) shows an electron diffraction pattern of an area covering the area in Fig. 3(a). The diffraction arcs, which spread for up to 15°, further confirm the small angle misorientation nature among the subgrains seen in Fig. 3(a).

Examination of the grain structures in the two-revolution and the nine-revolution HPT samples reveals significant difference from that of the one-revolution HPT sample. Subgrains with small angle subgrain boundaries are rare in the two-revolution HPT sample and are no longer seen in the nine-revolution sample, suggesting that, with the further deformation, grain orientation continued until all the subgrains had the same orientation and the subgrain structure disap-

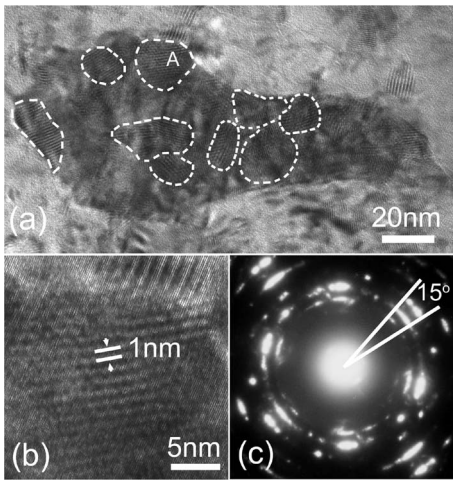

FIG. 3. (a) A TEM image of a grain with Moiré fringes. White dotted lines are drawn to circle Moiré fringe domains within which the fringes have the same orientation; (b) a magnified image of a domain marked with "A" in (a); (c) electron diffraction pattern of the area including (a).

peared to form a larger grain. The conversion of large angle grain boundaries to small angle grain boundaries is consistent with the observations of molecular dynamics simulations.[22,23] A typical TEM bright-field image of the nine-revolution HPT sample is shown in Fig. 4. The average grain sizes of the two samples are 124 and 132 nm, respectively. In fact, large grains did not grow further in the HPT process after two revolutions. The small average grain size difference between the two-revolution and the nine-revolution HPT samples is caused by the reduction in the number of small grains in the nine-revolution samples.

In the one-revolution sample, dislocations are seen with high density at subgrain boundaries (see Fig. 2) to accommodate the small angle misorientations between neighboring subgrains but are hardly seen within each subgrain, indicating that grain rotation plays a primary role in the early stage of the HPT process when the grains were the small initial grains (~22 nm). In contrast, high density of dislocations is observed in the grains in nine-revolution HPT sample and this can be easily seen through the strong contrast variation caused by the strain field around dislocations in grains, which are in a strong diffraction condition (i.e., the grains appear dark). An example can be seen from the grains with dark contrast in Fig. 4. The high density of dislocations found in the nine-revolution HPT sample indicates that dislocations play a primary role in accommodating the deformation process at this stage. In other words, during HPT at higher revolutions dislocation slip became the primary deformation mechanism, in which dislocation accumulation and dynamic recovery reached a dynamic balance. This dynamic balance determined the final grain size.

In summary, HPT induced grain growth in a bulk nc Ni-20 wt % Fe alloy with grains much smaller than 100 nm is primarily caused by grain rotation, which occurred three dimensionally. Grain boundary migration might have played a minor role during the grain growth. At the initial stage of the HPT process grain rotation first converted large angle grain boundaries to small angle subgrain boundaries, forming large grains with subgrains consisting of initial small grains. At a later stage of HPT, dislocation slip became the primary deformation mechanism, in which dislocation accumulation and dynamic recovery reached a dynamic balance. This dynamic balance determined the final grain size.

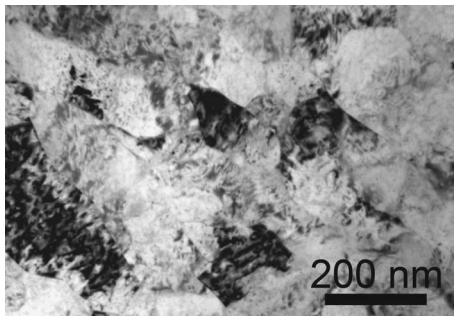

FIG. 4. A diffraction contrast image of the nine-revolution HPT sample.

The authors are grateful for scientific and technical input and support from the Australian Microscopy & Microanalysis Research Facility node at the University of Sydney. This project is financially supported by the Australian Research Council [Grant No. DP0772880 (Y.B.W., J.C.H, and X.Z.L.)], the LDRD program of Los Alamos National Laboratory (H.Q.L.), and the U.S. DOE IPP program (Y.T.Z.).

[1] R. Z. Valiev, R. K. Islamgaliev, and I. V. Alexandrov, Prog. Mater. Sci. **45**, 103 (2000).
[2] A. P. Zhilyaev and T. G. Langdon, Prog. Mater. Sci. **53**, 893 (2008).
[3] N. Hansen and X. Huang, Acta Mater. **46**, 1827 (1998).
[4] D. A. Hughes and N. Hansen, Acta Mater. **45**, 3871 (1997).
[5] X. Z. Liao, Y. H. Zhao, Y. T. Zhu, R. Z. Valiev, and D. V. Gunderov, J. Appl. Phys. **96**, 636 (2004).
[6] Y. S. Li, N. R. Tao, and K. Lu, Acta Mater. **56**, 230 (2008).
[7] Y. H. Zhao, Y. T. Zhu, X. Z. Liao, Z. Horita, and T. G. Langdon, Mater. Sci. Eng., A **463**, 22 (2007).
[8] F. A. Mohamed, Acta Mater. **51**, 4107 (2003).
[9] K. Zhang, J. R. Weertman, and J. A. Eastman, Appl. Phys. Lett. **87**, 061921 (2005).
[10] X. Z. Liao, A. R. Kilmanetov, R. Z. Valiev, H. S. Gao, X. D. Li, A. K. Mukherjee, J. F. Bingert, and Y. T. Zhu, Appl. Phys. Lett. **88**, 021909 (2006).
[11] G. J. Fan, L. F. Fu, H. Choo, P. K. Liaw, and N. D. Browning, Acta Mater. **54**, 4781 (2006).
[12] D. S. Gianola, S. Van Petegem, M. Legros, S. Brandstetter, H. Van Swygenhoven, and K. J. Hemker, Acta Mater. **54**, 2253 (2006).
[13] G. J. Fan, Y. D. Wang, L. F. Fu, H. Choo, P. K. Liaw, Y. Ren, and N. D. Browning, Appl. Phys. Lett. **88**, 171914 (2006).
[14] F. Sansoz and V. Dupont, Appl. Phys. Lett. **89**, 111901 (2006).
[15] D. Farkas, A. Froseth, and H. V. Swygenhoven, Scr. Mater. **55**, 695 (2006).
[16] J. C. M. Li, Phys. Rev. Lett. **96**, 215506 (2006).
[17] Z. W. Shan, E. A. Stach, J. M. K. Wiezorek, J. A. Knap, D. M. Follstaedt, and S. X. Mao, Science **305**, 654 (2004).
[18] Y. B. Wang, B. Q. Li, M. L. Sui, and S. X. Mao, Appl. Phys. Lett. **92**, 011903 (2008).
[19] M. W. Chen and X. Yan, Science **308**, 356c (2005).
[20] M. Legros, D. S. Gianola, and K. J. Hemker, Acta Mater. **56**, 3380 (2008).
[21] H. Q. Li and F. Ebrahimi, Mater. Sci. Eng., A **347**, 93 (2003).
[22] A. J. Haslam, D. Moldovan, V. Yamakov, D. Wolf, S. R. Phillpot, and H. Gleiter, Acta Mater. **51**, 2097 (2003).
[23] A. J. Haslam, S. R. Phillpot, D. Wolf, D. Moldovan, and H. Gleiter, Mater. Sci. Eng., A **318**, 293 (2001).